IMPROVED DIRECT TORQUE CONTROL USING KALMAN FILTER: APPLICATION TO A DOUBLY-FED MACHINE

Hamza Chaal and Milutin Jovanovic
School of Computing, Engineering and Information Sciences
Northumbria University, Newcastle upon Tyne, UK
Email: hamza.chaal@unn.ac.uk; milutin.jovanovic@unn.ac.uk

ABSTRACT
Direct Torque Control (DTC) has been extensively researched and applied during the last two decades. However, it has only first been applied to the Brushless Doubly-Fed Reluctance Machine (BDFRM) a few years ago in its basic form inheriting its intrinsic flux estimation problems that propagate throughout the algorithm and hence compromise the DTC performance. In this paper, we propose the use of Kalman Filter (KF) as an alternative to improve the estimation and consequently the control performance of the DTC. The KF is designed around a nominal model, but is shown to be reliable over the whole operating range of the BDFRM. Moreover, we use a modified robust exact differentiator based on Sliding Mode (SM) techniques to calculate the angular velocity from an angular position encoder. Computer simulations are meticulously designed to take into account real-world physical constraints and thus show illustrative supporting results as expected from an experimental setup.

KEYWORDS
Direct Torque Control, Kalman Filter, Robust Exact Differentiator, Brushless Doubly-Fed Reluctance Machine.

NOMENCLATURE

v_{pd}, v_{pq} primary direct and quadrature voltage components [V];

v_{sd}, v_{sq} secondary direct and quadrature voltage components [V];

i_{pd}, i_{pq} primary direct and quadrature current components [A];

i_{sd}, i_{sq} secondary direct and quadrature voltage components [A];

λ_{pd}, λ_{pq} primary direct and quadrature flux components [Wb];

λ_{sd}, λ_{sq} secondary direct and quadrature flux components [Wb];

ω angular velocity of reference frame [rad/sec];

ω_{rm} mechanical angular velocity of the shaft [rad/sec];

ω_r electrical angular velocity of the rotor [rad/sec];

$\omega_{p,s}$ primary and secondary winding frequencies [rad/sec];

P_r number of rotor poles (or the sum of the windings pole pairs);

L_p, L_s, L_m primary, secondary and mutual inductances of the windings [H];

R_p, R_s primary and secondary windings resistances [Ω];

T_e, T_l electromagnetic and load torque [Nm].

1 Introduction

The BDFRM has been the subject of extensive research during the last decade [1–6]. The motivation behind these generous efforts is largely explained by the tremendous potential for this machine in both motoring and generating modes. The BDFRM offers competitive performance to slip energy recovery induction machine drives while having a brushless and salient rotor. For a typical speed range of 2:1, the converter real power rating can be limited to about 25% of the machine rating [1–3]. Another interesting feature of the BDFRM is that it can function as a conventional induction machine, a synchronous machine, and a doubly excited induction machine [1]. For the same inverter ratings and assuming the same copper losses and active copper material, the BDFRM is able to produce approximately twice the output power of the Synchronous Reluctance Machine (SyncRel), using the maximum torque per inverter Ampere (MTPIA) control requirement. The absence of rotor windings also makes it more efficient and considerably easier to manufacture, model and control as compared to the Brushless Doubly-Fed Induction Machine (BDFIM) which has an additional winding on the rotor [3]. A further merit is the possibility of power-factor control, which is particularly useful when turbines are connected to weak grid systems.

The DTC algorithm has been developed more than two decades ago [7, 8] as an alternative to the conventional space vector or field oriented control for high-performance induction motor drives. The author of [7] replaced the complex control structure inherent with the latter by merely two hysteresis comparators and an optimum switching look-up table. Since then DTC gained a lot of interest among the research communities either in academia or industry alike due to its simplicity and high efficiency. For instance, ABB® adopted this approach and offers a range of DTC based products for variable speed applications. Furthermore, the literature is rich with DTC applications to single-excited AC machines. However, it reveals very little about applications to doubly-fed machines especially brushless.

DTC was first applied to the BDFRM in [9] and subsequently modified to a sensorless scheme in [5, 10]. It has been shown that DTC offers a good transient and steady state performance. Nonetheless, DTC has also disadvantages some of which are general to AC machines while oth-

ers are peculiar to the BDFRM. Voltage integration problems and associated flux estimation inaccuracies,as it happens with induction machines at low speeds, lie within the first category of DTC limitations. [5] overcomes this problem by using a different analytical expression that avoids secondary voltage integration but requires knowledge of the winding self inductances $L_{p,s}$ at the expense. A specific problem when applying DTC to the BDFRM of [5] is that the primary resistance R_p is large and hence the voltage drop across it cannot be neglected. Besides, for the MTPIA objective and in particular when the secondary current i_s is almost zero, even minor inaccuracies in the primary flux $\lambda_p$estimates can cause large inacceptable estimation errors in the secondary flux λ_s.

This paper is organized as follows; in section two we review the BDFRM model. In section three we develop a state observer to reconstruct the primary and secondary fluxes using Kalman Filter. Section four shows how the DTC is enhanced thanks to the new estimation algorithm. Section five illustrates the effectiveness of the proposed approach by simulations accounting for practical constraints. Finally in section six, we draw a conclusion about this work and mention some closing remarks.

2 Dynamic Model

In an arbitrary rotating reference frame, and using standard notation, the BDFRM dq-model is expressed as [4]:

$$\begin{cases} v_{pd} = R_p i_{pd} + \dot{\lambda}_{pd} - \omega\lambda_{pq} \\ v_{pq} = R_p i_{pq} + \dot{\lambda}_{pq} + \omega\lambda_{pd} \\ v_{sd} = R_s i_{sd} + \dot{\lambda}_{sd} - (\omega_r - \omega)\lambda_{sq} \\ v_{sq} = R_s i_{sq} + \dot{\lambda}_{sq} + (\omega_r - \omega)\lambda_{sd} \end{cases} \quad (1)$$

$$\begin{cases} \lambda_{pd} = L_p i_{pd} + L_m i_{sd} \\ \lambda_{pq} = L_p i_{pq} - L_m i_{sq} \\ \lambda_{sd} = L_s i_{sd} + L_m i_{pd} \\ \lambda_{sq} = L_s i_{sq} - L_m i_{pq} \end{cases} \quad (2)$$

Among many torque expressions for the machine, we chose the following due to control implications:

$$T_e = \frac{3P_r L_m}{2L_p}\left(\lambda_{pd} i_{sq} + \lambda_{pq} i_{sd}\right) \quad (3)$$

The torque is expressed as a function of the primary flux which is mainly constant (because the primary winding is fed with constant grid voltage and frequency) and the secondary currents which can be controlled by an inverter.

To complete the BDFRM model, we use a conventional mechanical equation for a single lumped inertia load neglecting friction components:

$$\frac{d\omega_{rm}}{dt} = \frac{1}{J}(T_e - T_l) \quad (4)$$

$$\omega_{rm} = \frac{w_p + w_s}{P_r} \quad (5)$$

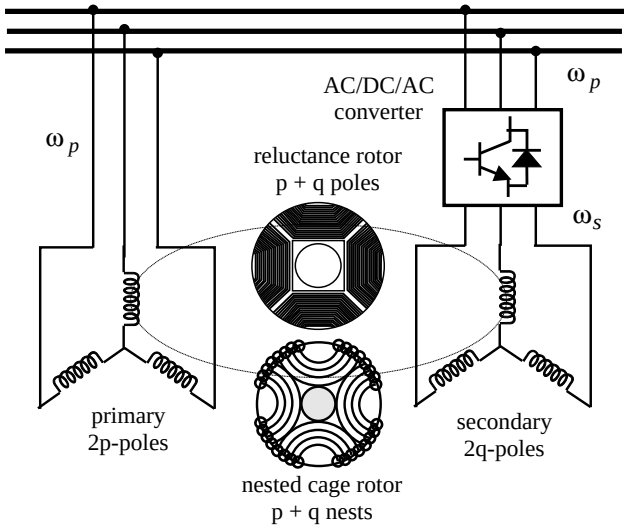

Figure 1. Structural diagram of BDFM drive with reluctance (BDFRM) and cage (BDFIM) rotors

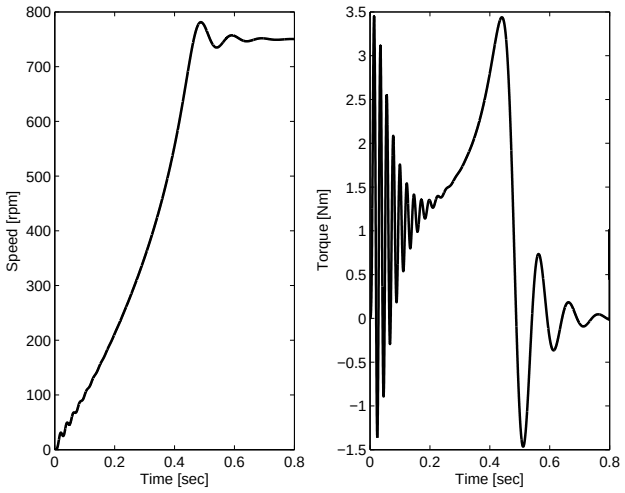

Figure 2. Starting transients for rotor speed (ω_{rm}) and torque (T_e)

Figure 1 depicts a schematic representation of the BDFRM setup as considered in this work. Figure 2 shows the rotor angular velocity, given by (5), and BDFRM torque during start-up to the synchronous speed of $\omega_{sync} = 750$rpm corresponding to (5) for $\omega_s = 0$ (when the secondary is DC fed). In the next figures we shall not show the starting performance again in order to focus on the doubly-fed operating mode.

3 Flux Estimation using Kalman Filter

First by manipulating (1) and (2) to eliminate the current variables and referring the model to the stationary frame (i.e. $\omega = 0$) we obtain:

$$\begin{cases} \dot{\lambda}_{pd} = v_{pd} - \mu R_p(L_m\lambda_{sd} - L_s\lambda_{pd}) \\ \dot{\lambda}_{pq} = v_{pq} + \mu R_p(L_s\lambda_{pq} + L_m\lambda_{sq}) \\ \dot{\lambda}_{sd} = v_{sd} + \omega_r\lambda_{sq} - \mu R_s(L_m\lambda_{pd} - L_p\lambda_{sd}) \\ \dot{\lambda}_{sq} = v_{sq} - \omega_r\lambda_{sd} + \mu R_s(L_m\lambda_{pq} + L_p\lambda_{sq}) \end{cases} \quad (6)$$

where: $\mu = (L_m^2 - L_pL_s)^{-1}$.

It is clear that the set of equations (6) represents a bilinear system. However, a physical constraint is imposed on the BDFRM due to the fact that it offers numerous virtues only if operated in a relatively narrow speed range around the synchronous speed i.e. $\omega_{rm} = \omega_{sync} \pm \Delta\omega_{rm}$, where; $\frac{\Delta\omega_{rm}}{\omega_{sync}} = 33.33\%$.

As suggested previously, typical ratio for limited speed range applications is: $\omega_{rm\_Max} = 2\omega_{rm\_Min}$ equivalent to $\omega_s = \frac{\omega_p}{3} \approx 17$Hz for $\omega_p = 50$Hz, which means that $\omega_{rm} = \omega_{sync} \pm 250$rpm. In this range, the power electronics required is only 20% the rating of the BDFRM [3]. This operational constraint can be exploited to simplify estimation and/or control schemes. In fact since $\omega_r = P_r\omega_{rm}$, then ω_r exhibits the same uncertainty as ω_{rm}. For developing the Kalman Filter system model we assume a constant nominal electrical velocity $\omega_r = \omega_n$ which results in a linear model of the standard form:

$$\dot{X} = AX + BU \quad (7)$$

where: $X = \begin{bmatrix}\lambda_{pd} & \lambda_{pq} & \lambda_{sd} & \lambda_{sq}\end{bmatrix}^T$, $B = I_{4\times4}$, $U = \begin{bmatrix}v_{pd} & v_{pq} & v_{sd} & v_{sq}\end{bmatrix}^T$, and

$$A = \begin{bmatrix} \mu R_pL_s & 0 & -\mu R_pL_m & 0 \\ 0 & \mu R_pL_s & 0 & \mu R_pL_m \\ -\mu R_sL_m & 0 & \mu R_sL_p & \omega_n \\ 0 & \mu R_sL_m & -\omega_n & \mu R_sL_p \end{bmatrix}.$$

The primary and secondary currents are measured quantities, therefore we rewrite (2) to get the output equation in the form $Y = CX$:

$$\begin{bmatrix} i_{pd} \\ i_{pq} \\ i_{sd} \\ i_{sq} \end{bmatrix} = \mu \begin{bmatrix} -L_s & 0 & L_m & 0 \\ 0 & -L_s & 0 & -L_m \\ L_m & 0 & -L_p & 0 \\ 0 & -L_m & 0 & -L_p \end{bmatrix} \begin{bmatrix} \lambda_{pd} \\ \lambda_{pq} \\ \lambda_{sd} \\ \lambda_{sq} \end{bmatrix} \quad (8)$$

To derive the discrete model we simply apply Euler's method with a sampling time h, which gives:

$$\begin{cases} X_{k+1} = A_kX_k + hBU_k + \xi \\ Y_k = CX_k + \eta \end{cases} \quad (9)$$

where: $A_k = \begin{bmatrix} a_1 & 0 & a_3 & 0 \\ 0 & a_1 & 0 & -a_3 \\ a_4 & 0 & a_2 & \omega_nh \\ 0 & -a_4 & -\omega_nh & a_2 \end{bmatrix}$,

$a_1 = 1 + \mu R_pL_sh$, $a_2 = 1 + \mu R_sL_ph$, $a_3 = -\mu R_pL_mh$, $a_4 = -\mu R_sL_mh$. ξ and η are introduced to account for the process and measurement noises. They are assumed identically independent zero mean white noises with respective first moments Q and R.

The KF equations are defined as follows [11]:

$$\begin{cases} \hat{X}_k = A_d\hat{X}_k + B_hU_k \\ P_k = A_dP_kA_d^T + Q_k \\ K_k = P_kC^T(CP_kC^T + R)^{-1} \\ \hat{X}_{k+1} = \hat{X}_k + K_k(Y_k - C\hat{X}_k) \\ P_{k+1} = (I - K_kC)P_k(I - K_kC)^T + K_kRK_k^T \end{cases} \quad (10)$$

where: K is the Kalman correction gain and P is the state prediction covariance.

Remark 1 *The last recursive equation in (10) may be simplified to $P_{k+1} = (I - K_kC)P_k$ as found in many texts. However, this would be at the cost of numeric stability and accuracy of the original expression.*

4 Improved Direct Torque Control

4.1 DTC strategy

For a Y-connected machine with an isolated neutral point (so that $i_c = -i_a - i_b$) and the "abc" phase sequence of the windings, we recall the expressions used in [5] for flux estimation given in complex form:

$$\underline{\lambda}_s = \lambda_s e^{j\theta_s} = L_s\underline{i}_s + \frac{\underline{\lambda}_p - L_p\underline{i}_p}{\underline{i}_s^*}\underline{i}_p^* \quad (11)$$

$$\underline{\lambda}_p = \lambda_p e^{j\theta_p} = \int \left(\underline{v}_p - R_p\underline{i}_p\right) dt \quad (12)$$

$$\underline{x} = x_a + j\frac{x_a + 2x_b}{\sqrt{3}}, \text{ where } x = i_p, i_s, v_p \quad (13)$$

This approach allows to avoid the well known voltage integration problems while estimating λ_s and $\theta_s = \frac{d\omega_s}{dt}$ (for sector identification). However, it is clear that (11) for estimating the secondary flux is not reliable when i_s is close to zero (which is the case for example when the machine is unloaded or during a transient response). Besides (12) and consequently (11) suffer high sensitivity to parameter inaccuracies in addition to the numerical stability issue. This has prevented the MTPIA control objective to be attained experimentally [5]. Therefore, using (11) is not recommended for real implementation, and a more robust estimation technique, like the one described in the previous section, is required. The same MTPIA secondary flux reference expression and inverter switching logic as in [5] can be applied.

4.2 Modified Robust Exact Differentiator

The classical way of making derivative of a physical measured quantity is to use a combination of an ideal differentiator and a low-pass filter. Such a linear differentiator inherently carries a time-delay proportional to its complexity. The author of [12] introduced a new method for Robust

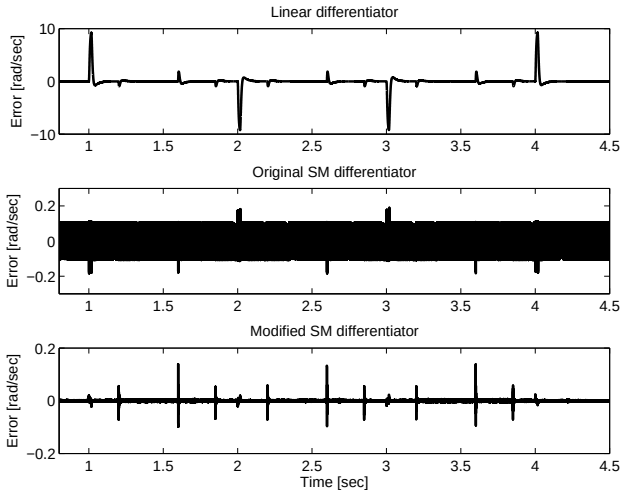

Figure 3. Speed differentiation errors

Exact Differentiation (RED) based on Sliding Mode (SM) techniques that we summarize here.

For a practical first-order robust exact differentiator, let the input signal $f(t)$ be a measurable locally bounded function that consist of a base signal having a derivative with Lipschitz's constant $C > 0$ and a noise. Consider the auxiliary equation $\dot{x} = u$ and apply a second order SM algorithm to steer x to $f(t)$. This results in the control law defined by (14):

$$\begin{cases} u = u_1 - \lambda\sqrt{|x - f(t)|}sign(x - f(t)) \\ u_1 = -\alpha sign(x - f(t)) \end{cases} \quad (14)$$

where $\alpha > 0, \lambda > 0$ and $u(t)$ is the output of the differentiator.

In order to reduce the chattering phenomenon we propose to use the approximation $tansig$ function ($tansig(x) = 2/(1 + exp(-\beta x)) - 1$) instead of the sharp $signum$ function. By this slight modification the performance of the RED is considerably improved in steady state in particular.

Now let's assess the performance of the RED against a linear one described by the transfer function $s/(\frac{s}{100\pi} + 1)^2$. Figure 3 shows a comparison of the differentiation errors obtained in a closed loop DTC scheme using a linear differentiator, the original RED and the modified RED with $\alpha = 10C$, $\lambda = 3\sqrt{C}$, $C = 2500$. The spikes appear at time instants where there is a reference change in the angular velocity or a change in the load torque. The modified SM based RED is more accurate and has in the worst situation error spikes with twice less amplitude than the original RED. The advantage of using the new SM differentiator is clearly demonstrated.

5 Simulation results

The key point in preparing for the experimental work is to make realistic simulations. In order to achieve this, we take the following measures:

1. We use the power electronic models readily available in Simulink/SimPowerSystems® library to reproduce the non-linear dynamics of the 3-phase diode rectifier, the braking chopper, the IGBT inverter bridge and the 3-phase voltage source.

2. To account for the current/voltage transducers effect, we inject high frequency measurement uncorrelated white noises to the ideal signals. Moreover, we corrupt the signals by unknown slowly varying DC offsets.

3. We assume that the only information available is the angular position provided by an incremental encoder. Some authors use linear observers in order to obtain the angular velocity. These kinds of observers are subject to criticism from many aspects, for instance the requirement of a torque transducer (or estimator) and unavoidable time delay. We adopt a real-time SM based RED instead, as explained earlier.

4. The computational expense has not been neglected. KF has been implemented using Embedded Matlab function to automatically generate efficient embedded C code and run simulations at compiled C speed. Besides we optimized the code by avoiding unnecessary matrix multiplications, minimizing the use of trigonometric functions and handling `single` precision variables.

The sampling frequency of the inner DTC loop including the power electronics has been set to 10 kHz, whereas the outer PI speed loop is updated at 1 kHz. The desired reference angular speed signal is set to cover all the operating range of the BDFRM. At the same time, we apply bounded unknown load torque step changes to challenge the improved control scheme. The experiment is set around a 2.5A, 415V, 50Hz BDFRM with the parameters found in [5].

5.1 KF vs conventional estimation

In order to reinforce the choice for KF as a state observer in contrast with the estimation method used in [5], we set up a simulation that implements the DTC using both estimation techniques. KF initial estimates are set to zero, and the covariance matrices to $P = 10 \times I$, $Q = 0.001 \times I$, $R = 0.1 \times I$. The comparison is made under ideal conditions, and the estimation errors of the secondary flux components are depicted in Figures 4 and 5. Employing KF is well justified given the crude estimation used in previous works and we now understand why MTPIA control objective was not achievable experimentally as mentioned earlier. In particular the conventional estimation method fails in regions where the machine is not loaded (secondary currents at zero) and where transients with low secondary currents occur. On the other hand, KF provides accurate estimates

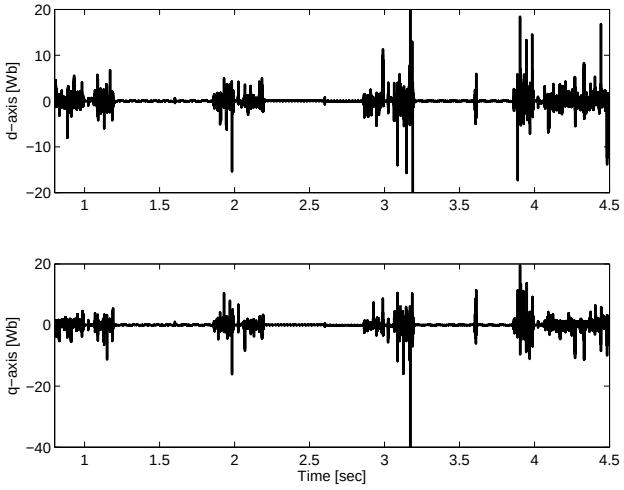

Figure 4. Secondary flux estimation error using conventional method

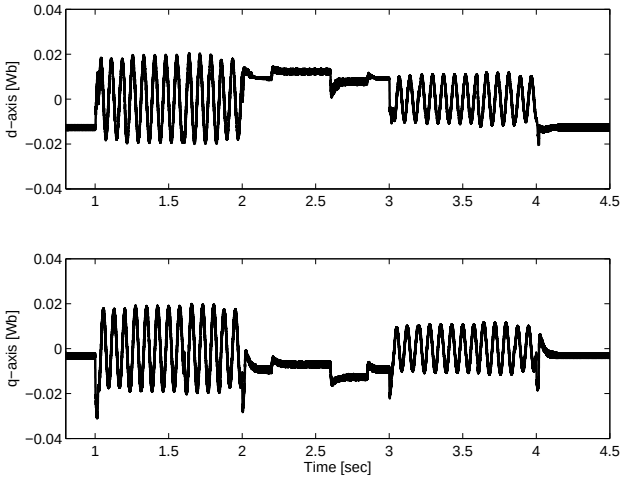

Figure 5. Secondary flux estimation error using KF

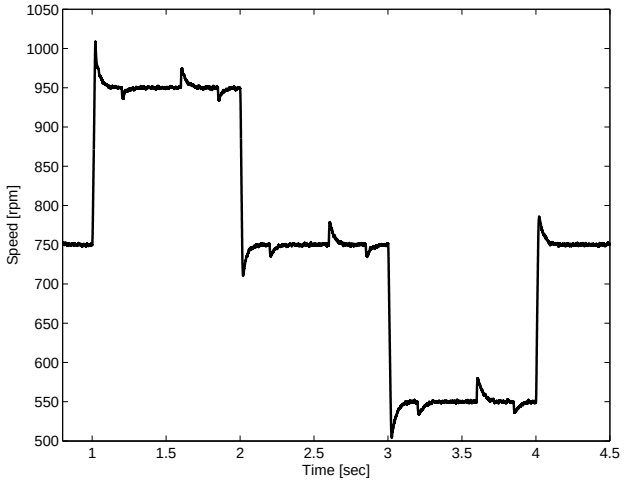

Figure 6. Speed tracking at different loads

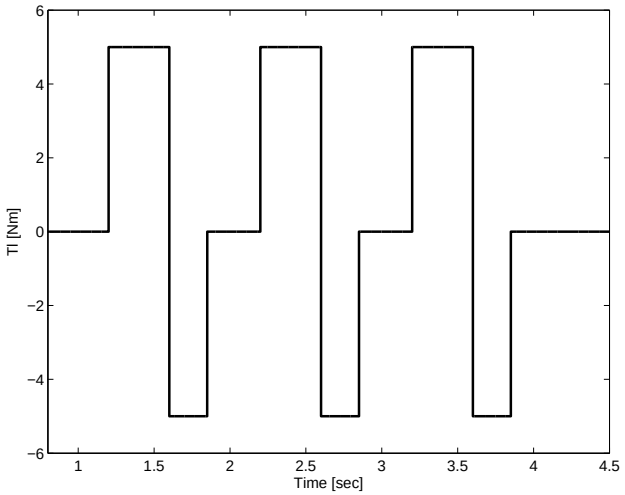

Figure 7. Applied load torque profile

despite the changing set point and load with minimum accuracy of 2%. Similar observations can be made for the primary flux estimation but respective waveforms are not shown for space reasons.

5.2 Testing the KF based DTC

Again for the sake of emulating a real-time situation, the BDFRM model is made uncertain by using immeasurable random disturbance inputs, introducing a random component into the state trajectory. The KF has no information about the disturbance input hence only a proper choice of Q matrix helps KF to converge to the real state trajectory. The larger the process noise covariance, the more KF makes use of the current measurements. However, the currents also are corrupted with noise and DC offset. We can accommodate the former by properly tuning R, whereas for the later, which has made the major obstacle for practical implementation in previous works, we do not even have to care about designing linear high-pass pre-filters; in fact KF estimates are virtually unaffected by the measurements DC offset. Figure 6 shows the tracking performance of the improved DTC under different loading conditions (Figure 7). The transient response is fast with respect to both speed and load torque changes. The steady state behavior is also very good.

Figure 8 shows the corresponding electromagnetic torque that compensates adequately for the changing load and desired speed. Yet, although the excellent tracking performance of the KF based DTC, the BDFRM torque is subject to high jitter exceeding the specified hysteresis band. This phenomenon is currently being investigated and is largely due to the consideration of practical effects such as the control sampling frequency limit imposed by computational requirements. Finally, Figure 9 outlines the d-q secondary currents with the q-axis current having a similar waveform to torque (Figure 8).

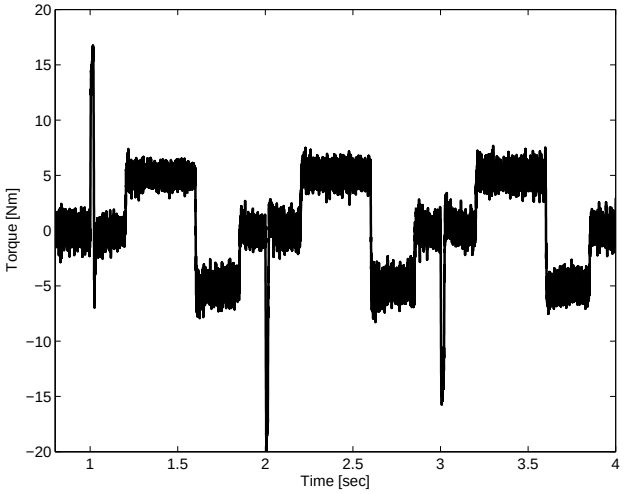

Figure 8. Electromagnetic torque (T_e)

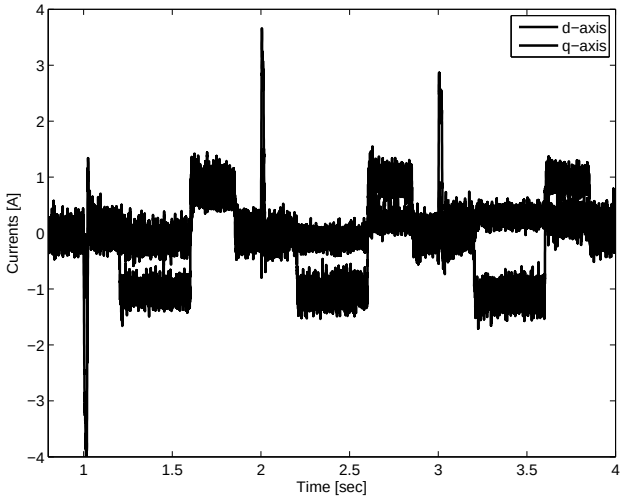

Figure 9. Secondary d-q currents in ω_s frame

6 Conclusion

In this paper we have reviewed the DTC proposed for the BDFRM addressing the weak points of the dedicated flux estimation method under the MTPIA conditions. In order to allow the MTPIA control strategy to be applied experimentally, we have suggested the use of Kalman Filter and showed its suitability for this task. Furthermore, we have used a modified RED based on SM techniques to calculate the angular velocity and demonstrated its superiority to conventional linear filters and the original RED. Realistic simulations accounting for practical constraints have been made to support the approach. The Matlab/Simulink results are more than promising and represent the necessary preliminary step for real-time implementation.

Acknowledgements

The authors would like to thank the EPSRC (Grant No. EP/F06148X/1) for financial support.

References

[1] R. E. Betz and M. G. Jovanovic, "The brushless doubly fed reluctance machine and the synchronous reluctance machine-a comparison," *IEEE Transactions on Industry Applications*, vol. 36, pp. 1103–1110, 2000.

[2] ——, "Theoretical analysis of control properties for the brushless doubly fed reluctance machine," *IEEE Transactions on Energy Conversion*, vol. 17, pp. 332–339, 2002.

[3] M. G. Jovanovic, R. E. Betz, and J. Yu, "The use of doubly fed reluctance machines for large pumps and wind turbines," *IEEE Transactions on Industry Applications*, vol. 38, pp. 1508– 1516, 2002.

[4] ——, "Introduction to the space vector modelling of the brushless doubly-fed reluctance machine," *Electric Power Components and Systems*, vol. 31, no. 8, pp. 729–755, 2003.

[5] M. G. Jovanovic, J. Yu, and E. Levi, "Encoderless direct torque controller for limited speed range applications of brushless doubly fed reluctance motors," *IEEE Transactions on Industry Applications*, vol. 42, no. 3, pp. 712–722, 2006.

[6] F. V. Puleston, "Variable structure control of a wind energy conversion system based on a brushless doubly fed reluctance generator," *IEEE Transactions on Energy Conversion*, vol. 22, no. 2, pp. 499–506, 2007.

[7] I. Takahashi and N. Toshihiko, "A new quick-response and high-efficiency control strategy of an induction motor," *IEEE Transactions on Industry Applications*, vol. 1A-22, no. 5, pp. 820–827, 1986.

[8] I. Takahashi and Y. Ohmori, "High performance direct torque control of an induction motor," *IEEE Transactions on Industry Applications*, vol. 25, no. 2, pp. 257–264, 1989.

[9] M. Jovanovic and J. Yu, "An optimal direct torque control strategy for brushless doubly-fed reluctance motors," *The Fifth International Conference on Power Electronics and Drive Systems*, 2003.

[10] M. G. Jovanovic, J. Yu, and E. Levi, "A doubly-fed reluctance motor drive with sensorless direct torque control." IEEE IEMDC, Madison, WI, 2003.

[11] Y. Bar-Shalom, X. R. Li, and T. Kirubarajan, *Estimation with Applications to Tracking and Navigation: Theory Algorithms and Software*, 1st ed. Wiley-Interscience, 2001.

[12] A. Levant, "Robust exact differentiation via sliding mode technique," *Automatica*, vol. 34, pp. 379–384, 1998.